

Unveiling the 2022 Southern Pakistan Flood Footprint: Insights from Sentinel Imagery and Land Deformation Analysis

Mohammad Sohail^{1,2,3}, Tianxing Chu^{2,3}

¹ Centre for Water Informatics & Technology, Lahore University of Management Sciences, Pakistan

² Department of Computer Science, Texas A&M University-Corpus Christi, USA

³ Conrad Blucher Institute for Surveying and Science, Texas A&M University-Corpus Christi, USA

ABSTRACT

Prior disaster management studies in the Indus flood plain of Pakistan have overlooked the potential of remote sensing for monitoring flood inundation zones over time. Still, there is a significant gap in understanding the impact of the devastating flood disaster on the land surface. Our research addresses this gap by utilizing multi-temporal Sentinel-1A, 2A, and ground-based validation surveys. This study uses the synthetic aperture radar interferometry (InSAR) technique to precisely characterize surface displacements resulting from the 2022 megaflood event in Pakistan. Our approach involves the analysis of SAR images captured from Sentinel-1A ascending passes, offering a comprehensive dataset for estimating land surface subsidence over the worst affected region in the Indus lower flood plain. The study's findings indicate a subsidence ranging from -229.82 to -7.84 mm. The urban land subsidence along the Indus River was particularly concerning, with some areas experiencing a substantial displacement of -215.26 mm. Significant subsidence, greater than -100 mm, affected 25.2% of the total study area. Agricultural land near the Indus River faced significant land displacement ranging from -180.82 to -7.84 mm due to the impact of floodwater. Additionally, regions with a maximum floodwater depth of 7 m exhibited higher land surface displacement. Floodwater depth was assessed using a Google Earth-based model. The primary causes of land displacement were excessive rainfall and the substantial flow of floodwater debris, requiring thorough attention from policymakers to ensure sustainable urban and agricultural development in the face of climate change.

Keywords: Climate change, Flood disaster, Indus Plain, SAR interferometry, Surface deformation, Land subsidence.

1. INTRODUCTION

The Intergovernmental Panel on Climate Change (IPCC) issued the Special Report on Extreme Events and Disasters (SREX), predicting rapid increases in extreme weather events during the twenty-first century [1], [2]. Climate change and global warming have become critical concerns for Pakistan,

particularly in relation to the growing frequency of extreme weather events [3], [4]. In recent years, Pakistan has experienced a notable increase in the occurrence of cloud bursts, leading to severe flooding with devastating consequences. The country is especially vulnerable to flooding, largely due to heavy summer monsoon precipitation [5]. The catastrophic flood in August 2022 had severe impact on the southern provinces of Pakistan, including Sindh and Baluchistan. This flood affected approximately one-third of the country, the world's fifth-most populous country, displacing an estimated 32 million people and resulting in economic losses exceeding \$30 billion [6], [7]. Recent studies on the spatial distribution of floodwaters and the evaluation of agricultural land degradation show that the flood inundated a total area of 26,252 km² across 21 districts, damaging approximately 1,307,102.8 hectares of agricultural land [7], [8].

Land subsidence poses a substantial threat and can severely damage infrastructure, including bridges, road networks, railways, and pipelines. Furthermore, it can result in significant stability problems in buildings in urban settlements [9]. To assess land subsidence, a variety of geodetic techniques, such as spirit leveling and global navigation satellite systems (GNSS), have been widely employed [10], [11]. However, these techniques are largely constrained by their limited coverage and sparse measurement distribution in space, making them inadequate for timely land deformation monitoring over large areas [12]. Interferometric synthetic aperture radar (InSAR) is a satellite-based land deformation monitoring technique that depends on measuring the phase difference between two radar images acquired at different epochs. InSAR has become a widely accepted and practical approach for tracking ground displacement events in global studies of land deformation [9], [13], [14], [15].

The objectives of this study are as follows: First, we used the Google Earth Engine (GEE)-based Floodwater Depth Estimation Tool along with Sentinel-2A imagery and a digital elevation model (DEM) to estimate floodwater depths to provide insights into flood extent and depth [8], [16]. Second, we applied InSAR technique using Sentinel-1A data to assess land subsidence, generating a spatial map highlighting areas

impacted by subsidence caused by the 2022 flood. Third, we evaluated the impact of land subsidence across the study area.

2. MATERIAL AND METHODS

2.1. Study area

The study focuses on the districts most severely impacted by 2022 flooding in southern Pakistan. Figure 1 illustrates the worst-affected regions, alongside a map of the land use and land cover within the study area. The flood extent maps indicate that the following districts experienced significant damage: Kashmore, Nasirabad, Jacobabad, Sholapur, Sukkur, Shikarpur, Larkana, and Thul. At the peak of the flooding, water depths reached up to 7 m, resulting in the inundation of approximately 66 km², primarily in the northern and western parts of the study area [8]. Houses and other infrastructure were submerged after heavy rains and flood during the monsoon season, as shown in Figure 1.

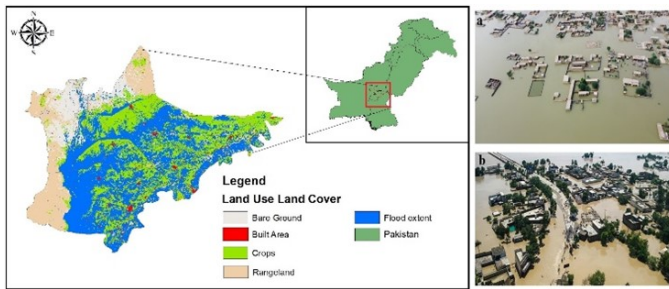


Fig. 1. The extent of floodwater over agricultural and urban land in the worst affected district in southern Pakistan. Photos (a) and (b) show the flood water over the Larkana and Sukkur districts in Pakistan's south and western regions

2.2. Data collection and pre-processing

This research used multispectral instrument (MSI) data from Sentinel-2A and SAR data from Sentinel-1A before (June 2022) and after (from September 2022 to January 2023) the flood. The details of the satellite data used in the study are provided in Table 1. The visible bands and near-infrared (NIR) from Sentinel-2A were used to calculate the water index and conduct flood inundation analysis. Normalized difference water index (NDWI) was computed using the green and NIR bands. This index efficiently filters out soil and vegetation data, making water more distinguishable in the image [8].

The floodwater depth estimation model incorporated floodwater extent and DEM data to determine the floodwater depth [16]. On the other hand, Sentinel-1A utilizes C-band to illuminate the Earth's surface, with backscatter recorded in vertical-horizontal (VH) and vertical-vertical (VV) polarizations. In this research, we utilized Sentinel-1 imagery from

Table 1. This explains the details of the satellite data used in the study.

Data	Description	Dates
Sentinel 1A (SAR)	IW-SLC, VV, Ascending	June 2022 (Pre-flood)
DEM	SRTM (30 m)	to
Sentinel 2 (MSI)	Bands (2, 3, 4, 8, and 11)	January 2023 (Post-flood)

the European Space Agency (ESA) as the primary dataset for monitoring land surface deformation. The DEM data was acquired from NASA's Shuttle Radar Topography Mission (SRTM). Table 1 shows the datasets used in this study. The Sentinel-1A satellite was designed for environmental monitoring and revisits the same area every 12 days [17], [18].

Differential interferometry (DInSAR) can identify displacements in the line of sight direction with centimeter-level accuracy [13]. Furthermore, applying temporal and spatial filtering can enhance the precision of deformation measurements. In this InSAR process, we chose the image before the 2022 flood as the master image for co-registration and interferogram formation. An interferogram is generated by cross-multiplying the master image with the complex conjugate of the slave image. The amplitudes of both the master and slave images are multiplied [15]. Equation (1) gives the multi-repeat-pass interferometric phase at the study area,

$$\phi_{total} = \phi_{flat} + \phi_{topo} + \phi_{atm} + \phi_{orb} + \phi_{noise} + \phi_{def} \quad (1)$$

where ϕ_{flat} defines the flat earth phase, ϕ_{topo} is the phase caused by the topography, ϕ_{atm} is the phase contributed by the atmosphere, ϕ_{orb} is due to orbital errors. ϕ_{noise} refers to the noise or artifacts, and the last ϕ_{def} corresponds to the deformation phase, which is the phase shift caused by actual surface displacement. More specifically,

$$\phi_{total} = \frac{4\pi}{\lambda} \frac{B_{\parallel}}{R \tan \theta} + \frac{4\pi}{\lambda} \frac{B_{\perp}}{R_0 \sin \theta} \Delta h + \frac{4\pi}{\lambda} \Delta D + \phi_{noise} + \phi_{def} \quad (2)$$

in the equation (2), λ represents the wavelength, B_{\parallel} is the perpendicular baseline, B_{\perp} is the perpendicular baseline, R signifies the slant range, and θ denotes the incident angle. Furthermore, $\Delta\phi_{def}$ represents the deformation differential phase, Δh represents the change in height or displacement of the surface, ΔD indicates the non-linear deformation component, and $\Delta\phi_{noise}$ defines the noise term in the SAR phase [19]. Equation (3) expresses the relationship between the change in phase $\Delta\phi$ and the displacement ΔR ,

$$\Delta\phi = \frac{4\pi}{\lambda} \Delta R \quad (3)$$

where Equation (3) expresses the relationship between the phase shift $\Delta\phi$ and the displacement ΔR . Since the displacement can be due to surface deformation caused by a flood, we

can analyze surface subsidence over the study area by measuring phase changes and using this equation. After the subswath selection, the data was split, and a process known as "deburst" was applied to eliminate potential radiometric errors. This was necessary because the IW SLC product was acquired in a series of bursts, and these radiometric errors could accumulate. The debursted imagery was subsequently calibrated to establish a direct relationship between the pixel values in the image and the backscatter received after interacting with the observed target. Once the interferogram was generated, a coherence map was produced. Coherence measures the similarity between the master and slave images with values spanning from 0 to 1. Values approaching 1 signify a substantial similarity, commonly found in permanent features like built-up corner points [18]. A reference DEM is then used to remove the topographically induced phase from the interferogram, isolating deformation signals from elevation-related phase variations [20]. For displacement estimation, the phase undergoes a cycle that resets to zero each time it completes a 2 phase cycle. It is crucial to resolve this ambiguity by unwrapping the phase and eliminating the 2 phase cycles [21], [22]. The unwrapped phase is subsequently employed for estimating and mapping displacement using Equation (4) below,

$$\text{Displacement} = -\frac{\phi_{\text{uwp}}\lambda}{4\pi \cos \theta} \quad (4)$$

where ϕ_{uwp} is the unwrapped phase, λ is the SAR wavelength, and θ is the SAR signal's incidence angle.

3. RESULTS AND DISCUSSION

The floodwater depth maps (Figure 2) highlight the districts most affected by the flooding, including Jacobabad, Shikarpur, Sukkur, Larkana, and Thul. Initially, the maximum floodwater depths reached up to 7 m. However, most of the affected area experienced flooding at a mean depth of approximately 2 m.

To evaluate the changes in the land surface caused by the flood, a final land deformation map was generated overlaid with the water depth data. The results reveal that the vertical deformation across the study area ranged from -229.82 to -7.84 mm following the flood event. These negative values indicate downward movement of the Earth's surface relative to the SAR sensor. A subsidence pattern of high spatial variability can be observed in Figure 3, particularly in agricultural land, such as the Jacobabad, Shikarpur, and Sukkur districts along the riverbanks. In urban regions, land subsidence was most pronounced along the riverbanks, with a maximum subsidence of -210.26 mm observed from the northern to the southern directions. As shown in Figure 3, the negative values reflect subsidence in areas adjacent to the river, indicating downward movement of the land. Land subsidence in the

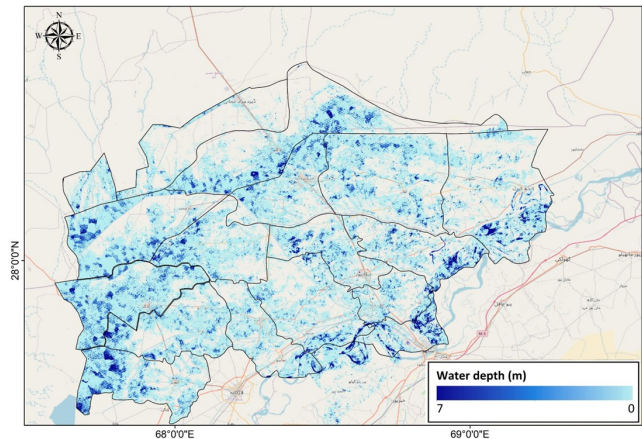


Fig. 2. The spatial distribution of water depth (m) on September 5, 2022, at various locations within the severely impacted districts.

western direction was relatively lower, with a maximum displacement of up to -124 mm.

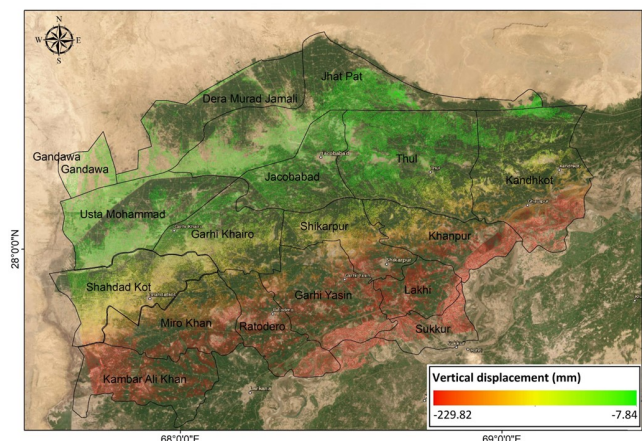


Fig. 3. Land subsidence across the study area following the mega flood 2022. The color ramp, ranging from green to red, illustrates the extent of subsidence in the vertical direction. Green indicates low subsidence and red represents high deformation.

We divided the study area into three classes: high, moderate, and low. High subsidence, defined as displacements greater than -100 mm, affects 25.2% of the total area. Moderate subsidence, ranging from -25 mm to -100 mm, was observed in 44.8% of the study region. In contrast, areas experiencing minimal or no subsidence account for 30% of the study area, as shown in Figure 4.

Regarding flood extent, the results indicate that up to 58% of the area was inundated with floodwaters reaching depths up to 2 m. The deepest floodwaters reached up to 7 m and covered less than 3% of the total area. Additionally, according

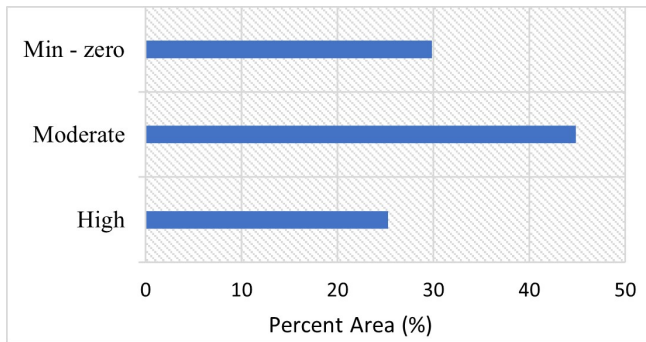


Fig. 4. The severity of land subsidence vs. the percentage of area affected.

to Figures 2 and 3, the correlation between water depth and land subsidence was observed, with areas of deeper flooding exhibiting more land subsidence.

Although there is a lack of GPS-based and in-situ data on land subsidence monitoring across the study area, an analysis using synthetic aperture radar (SAR) data, coupled with field investigations, suggests that land subsidence in the affected regions is likely linked to the substantial flow of floodwater debris and influenced by local soil geomorphology. In addition, the movement of heavy debris and boulders within floodwaters can lead to changes in the land surface, including subsidence. This process can further exacerbate flooding, particularly in the surrounding villages of the Sukkur, Larkana, and Thul districts. The mean water depth (in meters) was recorded at four locations in the worst-affected districts, with ground validation conducted at these sites on November 25–26, 2022, as shown in Figure 5. This validation provides an essential comparison for assessing the accuracy of the estimated water depths in the affected areas.

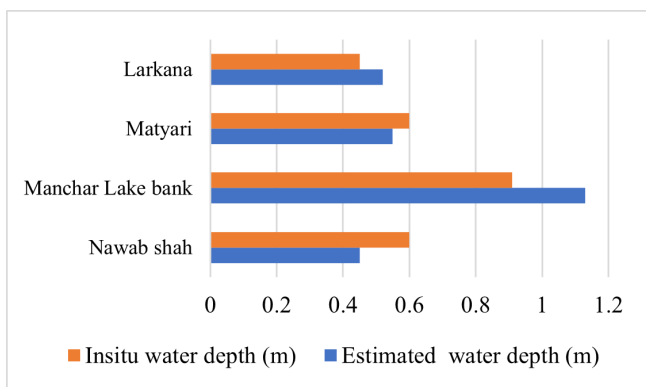


Fig. 5. Mean water depth (m) at four locations in the worst-affected districts, with ground validation conducted on November 25–26, 2022.

The accuracy analysis reveals that the estimated water depths exceed the in-situ measurements at some locations,

suggesting a slight overestimation. Nonetheless, this difference is relatively minor and indicates reasonable accuracy was achieved. For instance, at the Manchar Lake Bank, a discrepancy is observed, suggesting an overestimation of floodwater depths in this region. In contrast, the Matyari district demonstrates high accuracy in estimating floodwater depth relative to the in-situ measurements.

4. CONCLUSION

The 2022 flood almost submerged most of the agricultural and urban land of the southern Indus plain of Pakistan. This study utilized multi-temporal Sentinel-1A and Sentinel-2A imagery and ground-based validation surveys to analyze severely affected regions of the lower Indus floodplain. The results from the Google Earth-based water depth estimation indicated that the deepest floodwaters reached up to 7 m and covered up to 3% of the total study area. Land surface subsidence resulting from the 2022 flood were assessed by using InSAR techniques, indicating a range of subsidence from -229.82 mm to -7.84 mm. The study area was classified into three subsidence categories: high, moderate, and low. High subsidence the value is greater than -100 mm affects 25.2%, moderate subsidence (-25 mm to -100 mm) covers 44.8%, and minimal or no subsidence accounts for 30% of the total study area. Significant subsidence was noted in urban settlements in the eastern and southern regions of the study area. Nevertheless, there is still much work to be done in developing an early warning system for disaster resilience and risk reduction. Internet of things (IoT) and machine learning models can be linked with satellite data as early warning systems for disasters. This study emphasized that land subsidence can pose a substantial risk to urban structures and infrastructure to the affected areas, necessitating attention from policymakers.

5. REFERENCES

- [1] A. Al Mamun, A. R. M. T. Islam, G. M. Alam, M. N. I. Sarker, M. O. Erdiaw-Kwasie, H. Bhandari, and J. Mallick, “Livelihood vulnerability of char land communities to climate change and natural hazards in bangladesh: an application of livelihood vulnerability index,” *Natural Hazards*, vol. 115, no. 2, pp. 1411–1437, 2023.
- [2] D. Poursanidis and N. Chrysoulakis, “Remote sensing, natural hazards and the contribution of esa sentinels missions,” *Remote Sensing Applications: Society and Environment*, vol. 6, pp. 25–38, 2017.
- [3] M. Sohail, Z. Ahmad, and A. Muhammad, “Catchment-level estimation of snow depth using sentinel-1 and ground sensor validation in the upper indus basin,” in *IGARSS 2022 - 2022 IEEE International Geoscience and Remote Sensing Symposium*, pp. 4260–4263, 2022.

- [4] M. Sohail, S. S. F. Ali, E. Fatima, and D. A. Nawaz, "Spatio-temporal analysis of land use dynamics and its potential implications on land surface temperature in lahore district, punjab, pakistan," *The International Archives of the Photogrammetry, Remote Sensing and Spatial Information Sciences*, vol. XLIII-B3-2021, pp. 359–367, 2021.
- [5] A. Ali, "Indus basin floods: Mechanisms, impacts, and management," Tech. Rep. assistance., 1550.
- [6] N. JS, A. P. Kushwaha, R. Singh, I. Malik, U. Vegad, S. Dangar, S. Mahto, H. Solanki, D. Chuphal, and V. Mishra, "The pakistan flood of august 2022: causes and implications," in *AGU Fall Meeting Abstracts*, vol. 2022, pp. U23D–05, 2022.
- [7] F. M. Qamer, S. Abbas, B. Ahmad, A. Hussain, A. Salman, S. Muhammad, M. Nawaz, S. Shrestha, B. Iqbal, and S. Thapa, "A framework for multi-sensor satellite data to evaluate crop production losses: the case study of 2022 pakistan floods," *Scientific Reports*, vol. 13, no. 1, p. 4240, 2023.
- [8] M. Sohail and A. Muhammad, "Assessment of the 2022 flood disaster in pakistan's lower indus plain using sar and optical remote sensing," in *IGARSS 2023-2023 IEEE International Geoscience and Remote Sensing Symposium*, pp. 2173–2176, IEEE, 2023.
- [9] L. Solari, M. Del Soldato, S. Bianchini, A. Ciampalini, P. Ezquerro, R. Montalti, F. Raspini, and S. Moretti, "From ers 1/2 to sentinel-1: subsidence monitoring in italy in the last two decades," *Frontiers in Earth Science*, vol. 6, p. 149, 2018.
- [10] S. Shahbazi, Z. Mousavi, and A. Rezaei, "Constraints on the hydrogeological properties and land subsidence through gnss and insar measurements and well data in salmas plain, northwest of urmia lake, iran," *Hydrogeology Journal*, vol. 30, no. 2, pp. 533–555, 2022.
- [11] V. K. Maurya, R. Dwivedi, and T. R. Martha, "Site scale landslide deformation and strain analysis using mt-insar and gnss approach—a case study," *Advances in Space Research*, vol. 70, no. 12, pp. 3932–3947, 2022.
- [12] M. Nguyen, Y. N. Lin, Q. C. Tran, C.-F. Ni, Y.-C. Chan, K.-H. Tseng, and C.-P. Chang, "Assessment of long-term ground subsidence and groundwater depletion in hanoi, vietnam," *Engineering Geology*, vol. 299, p. 106555, 2022.
- [13] S. Alatza, I. Papoutsis, D. Paradissis, C. Kontoes, and G. A. Papadopoulos, "Multi-temporal insar analysis for monitoring ground deformation in amorgos island, greece," *Sensors*, vol. 20, no. 2, p. 338, 2020.
- [14] P. Yastika, N. Shimizu, and H. Abidin, "Monitoring of long-term land subsidence from 2003 to 2017 in coastal area of semarang, indonesia by sbas dinsar analyses using envisat-asar, alos-palsar, and sentinel-1a sar data," *Advances in Space Research*, vol. 63, no. 5, pp. 1719–1736, 2019.
- [15] A. Ciampalini, L. Solari, R. Giannecchini, Y. Galanti, and S. Moretti, "Evaluation of subsidence induced by long-lasting buildings load using insar technique and geotechnical data: The case study of a freight terminal (tuscan, italy)," *International Journal of Applied Earth Observation and Geoinformation*, vol. 82, p. 101925, 2019.
- [16] S. Cohen, A. Raney, D. Munasinghe, J. D. Loftis, A. Molthan, J. Bell, L. Rogers, J. Galantowicz, G. R. Brakenridge, A. J. Kettner, *et al.*, "The floodwater depth estimation tool (fwDET v2. 0) for improved remote sensing analysis of coastal flooding," *Natural Hazards and Earth System Sciences*, vol. 19, no. 9, pp. 2053–2065, 2019.
- [17] M. A. Aziz, M. Moniruzzaman, A. Tripathi, M. I. Hossain, S. Ahmed, K. R. Rahaman, F. Rahman, and R. Ahmed, "Delineating flood zones upon employing synthetic aperture data for the 2020 flood in bangladesh," *Earth Systems and Environment*, vol. 6, no. 3, pp. 733–743, 2022.
- [18] A. Tripathi, M. Moniruzzaman, A. R. Reshi, K. Malik, R. K. Tiwari, C. Bhatt, and K. R. Rahaman, "Chamoli flash floods of 7th february 2021 and recent deformation: A psinsar and deep learning neural network (dlNN) based perspective," *Natural Hazards Research*, vol. 3, no. 2, pp. 146–154, 2023.
- [19] Y. Gao, W. Yang, R. Guo, and L. Jiang, "Remote sensing monitoring and analysis of jinwuco lateral moraine landslide-glacial lake outburst in southeast tibet," *Remote Sensing*, vol. 15, no. 6, p. 1475, 2023.
- [20] K. Dai, Z. Li, R. Tomás, G. Liu, B. Yu, X. Wang, H. Cheng, J. Chen, and J. Stockamp, "Monitoring activity at the daguangbao mega-landslide (china) using sentinel-1 tops time series interferometry," *Remote Sensing of Environment*, vol. 186, pp. 501–513, 2016.
- [21] R. M. Goldstein and C. L. Werner, "Radar interferogram filtering for geophysical applications," *Geophysical research letters*, vol. 25, no. 21, pp. 4035–4038, 1998.
- [22] H. Jiang, T. Balz, F. Cigna, and D. Tapete, "Land subsidence in wuhan revealed using a non-linear psinsar approach with long time series of cosmo-skymed sar data," *Remote Sensing*, vol. 13, no. 7, p. 1256, 2021.